Localization of Fascin to Dendritic Protrusions Regulates Postsynaptic Plasticity

[1,2,3] James Q Zheng, [1] Shuristeen Joubert, [1] Carlos Gonzalez-Islas, [4] Yuki Ogawa, [1] Abhishek Poddar, [1] Arjolyn B Penas, [1] Enyu Liu, [1] Peter Wenner and [1] Kenneth R Myers

1. Department of Cell Biology, Emory University School of Medicine, Atlanta, GA 30322

2. Department of Neurology, Emory University School of Medicine, Atlanta, GA 30322

3. Center for Neurodegenerative Disease, Emory University School of Medicine, Atlanta, GA 30322

4. Department of Biological Sciences, McCausland College of Arts and Sciences, University of South Carolina, Columbia, SC 29208

Keywords: Actin cytoskeleton, dendrite, synapse, dendritic spines, actin bundling

Abstract: 152, *Introduction:* 611, *Results and discussion:* 1936, *Figures:* 3, Supplemental figures: 3

Correspondence: James Zheng, PhD, Department of Cell Biology, 615 Michael Street, Atlanta, Georgia 30322, USA. Email: james.zheng@emory.edu

Acknowledgements: We would like to thank Dr. Matthew N Rasband at Baylor College of Medicine for facilitating and supporting the development of the CRISPR constructs and plasmids for this study. This research is supported in part by research grants from the NIH to JQZ (MH133798, NS132393), and a Whitehall Foundation research grant to KRM (2023-08-069). This work was also supported by the Emory University Emory Integrated Cellular Imaging Core Facility (RRID:SCR_023534). The content is solely the responsibility of the authors and does not necessarily reflect the official views of the National Institute of Health.

Author contributions: JQZ conceptualized and initiated the project, as well as designed and conducted most of the experiments and data analysis. SJ performed the imaging and biochemical analyses on different fascin antibodies and knockout efficacy. CGI and PW helped with the electrophysiology recordings. YO helped with the CRISPR design and validation of fascin KO and KI constructs. AP helped with spine analysis. ABP performed fascin immunostaining. EL helped with spine analysis of the control and fascin KO groups. KRM helped with experimental design, molecular biology, and image analysis, and worked with JQZ on the manuscript writing.

Abstract

The Fascin family of actin-bundling proteins organizes actin filaments (F-actin) into tightly packed bundles that drive dynamic membrane protrusions such as filopodia. In neurons, fascin has been thought to primarily function in axons, as previous studies reported its absence from dendritic filopodia and spines. Here, we demonstrate that fascin is both present and functionally important in dendritic compartments. Using optimized immunocytochemistry and CRISPR-based endogenous tagging of fascin1 in cultured hippocampal neurons, we show that fascin localizes to developing dendritic filopodia and is enriched in mature dendritic spines. Super-resolution imaging further reveals that fascin is organized into discrete nanoscale foci within spine heads, but not the spine neck. Finally, we show that CRISPR-mediated knockout of fascin1 in mature hippocampal neurons impairs synaptic potentiation, without affecting baseline excitatory synaptic transmission. Together, our findings uncover a previously overlooked aspect of actin organization in dendritic spines and establish fascin as a critical regulator of postsynaptic plasticity.

Summary Statement

The actin bundling protein fascin localizes to dendritic filopodia and spines, where it regulates activity-dependent synaptic plasticity.

Introduction

Chemical synapses are specialized sites of connection that enable neuronal communication underlying sensorimotor behaviors, learning, memory, and cognition. Synapses are composed of pre- and post-synaptic structures specialized for neurotransmitter release and reception, respectively. These structures are highly plastic, undergoing both functional and structural modifications in response to activity (Bin Ibrahim et al., 2022; Ge et al., 2010; Malenka, 1994). This includes alterations in postsynaptic surface neurotransmitter receptors and presynaptic neurotransmitter release probability (Anggono and Huganir, 2012; Benke and Traynelis, 2019; Bosch and Hayashi, 2012; Citri and Malenka, 2008; Monday and Castillo, 2017). Synaptic plasticity represents the cellular basis for learning and memory (Martin et al., 2000; Takeuchi et al., 2014), and its disruption contributes to a wide range of neurological disorders (Lima Caldeira et al., 2019; Nishiyama, 2019; Stefen et al., 2016; Walker and Herskowitz, 2021).

Most excitatory synapses in the vertebrate brain reside on dendritic spines, which are tiny actin-rich protrusions that concentrate postsynaptic components for effective excitatory synaptic transmission (Chidambaram et al., 2019; Hotulainen and Hoogenraad, 2010; Nimchinsky et al., 2002). Spines undergo structural changes in shape and size during development and synaptic plasticity that are strongly associated with learning, aging, and neurodegenerative diseases (Lima Caldeira et al., 2019; Nishiyama, 2019; Stefen et al., 2016; Walker and Herskowitz, 2021). Dendritic filopodia, which act as spine and synaptic precursors, are thin actin-rich structures that sample the neuropil for axonal partners before stabilizing upon contact (Lohmann and

Bonhoeffer, 2008; Spence et al., 2016). Both dendritic filopodia and spines depend upon the actin cytoskeleton for their formation, remodeling, and maintenance (Bucher et al., 2020; Hotulainen and Hoogenraad, 2010; Lei et al., 2016; Okabe, 2020). Unlike conventional filopodia, which contain tightly bundled unipolar arrays of parallel actin filaments, dendritic filopodia and thin spine necks contain branched and straight actin filaments of mixed polarity that do not form tight bundles (Hotulainen et al., 2009; Korobova and Svitkina, 2010). These networks are organized and remodeled by a large number of actin binding proteins (ABPs) (Chhabra and Higgs, 2007; Pollard et al., 2000; Pollard and Borisy, 2003; Revenu et al., 2004). During structural long-term potentiation (sLTP), distinct sets of ABPs sequentially reorganize, stabilize, and consolidate the actin network in individual spines (Bosch et al., 2014). Actin-bundling proteins are essential for the reorganization and stabilization steps during sLTP, although the specific ABPs and their precise roles in these processes remain unclear (Bosch et al., 2014).

Fascin is a highly conserved actin-bundling protein best known for generating tightly packed filamentous actin (F-actin) bundles in dynamic membrane protrusions such as filopodia and invadopodia (Adams, 2004; Jansen et al., 2011; Krey et al., 2016; Li et al., 2010; Vignjevic et al., 2006). In neurons, fascin has been mostly studied in developing axons, where it localizes to growth cone filopodia and contributes to axon elongation and guidance (Cohan et al., 2001; Hardin et al., 2025; Sasaki et al., 1996). However, fascin is reportedly absent from dendritic filopodia and spines (Korobova and Svitkina, 2010; Parker et al., 2023), leading to the prevailing view that fascin plays no role in postsynaptic actin organization or plasticity. In this study, we challenge this model by

showing that fascin is present and functionally important in dendritic compartments. Using a combination of confocal microscopy, super-resolution imaging, and CRISPR/Cas9 gene editing, we show that fascin is enriched in dendritic filopodia and mature spines, where it forms discrete nanoscale foci within spine heads. Functionally, we demonstrate that CRISPR-based knockout of fascin1 in mature hippocampal neurons impairs activity-dependent synaptic potentiation without affecting baseline neurotransmission. These findings reveal an unexpected role for fascin in the modulation of the dendritic actin cytoskeleton and establish fascin as a critical regulator of synaptic plasticity.

Materials and Methods

Cell culture

Dissociated primary hippocampal neuron cultures were prepared as previously described (Gu et al., 2010). Briefly, 18.5-day-old embryos were collected from timed-pregnant Sprague Dawley rats (Charles River Laboratories), and hippocampi were dissected in ice-cold Hank's Balanced Salt Solution (HBSS). Hippocampi were pooled together, trypsinized for 12 minutes, briefly incubated in 20% fetal bovine serum, and plated on 25 mm acid-washed glass coverslips coated with 100 µg/ml poly-L-lysine (P2636; Sigma-Aldrich) at a density of approximately 300,000 cells per 35 mm dish. Hippocampal neurons were cultured in Neurobasal medium (21103049; Gibco) supplemented with B-27 (17504044; Gibco), penicillin/streptomycin (30002CI; ThermoFisher), and GlutaMax (35050061; Gibco), and fed ½ volume of fresh medium every 7 days post-plating. Animal care and use was conducted following National Institutes of Health guidelines, and procedures were approved by the Institutional Animal Care and Use Committee at Emory University.

Low density hippocampal culture was prepared using a feeder layer of cortical neurons according to the previously published method (Lu et al., 2016). Here, hippocampal neurons were plated on poly-L-lysine-coated 25 mm glass coverslips at a density of 25,000 cells per well in a 6-well culture plate. In a separate 6-well culture plate, several small paraffin wax dots ~2 mm in diameter and ~1 mm in height were planted on the bottom of each well, serving as spacers. After coating the bottom of each well with 100 µg/ml poly-L-lysine, cortical neurons from the same embryonic brains were plated at a density of 400,000 cells per well. After 24 h in culture, the coverslip with low-

density hippocampal neurons was removed from its plate and placed in the 6-well plate of cortical neurons with the hippocampal neurons facing down towards the cortical neurons. Weekly ½ volume medium changes were carried out as described above.

The mouse neuroblastoma cell line, Cath.-a-differentiated (CAD) (Qi et al., 1997), was maintained in DMEM/F12 (10-092-CV; Corning) supplemented with 8% fetal bovine serum (Atlanta Biologicals) and 1% Penicillin/Streptomycin (Invitrogen). To obtain CAD cells with elaborated lamellipodia and filopodia, we re-suspended the cells and plated them on laminin-coated (20 µg/ml) glass coverslips for 2-3 hours at 37 ^{o}C before fixation/immunofluorescence or live cell imaging (Pollitt et al., 2020; Vitriol et al., 2015).

Transient transfection and AAV-based transduction

To transiently express GFP-tagged proteins in CAD cells, X-tremeGENE HP DNA transfection reagent was used to transiently express exogenous genes (Pollitt et al., 2020; Vitriol et al., 2015).

To endogenously tag fascin1 in cultured hippocampal neurons, we utilized the Homology-Independent Universal Genome Engineering (HiUGE) method (Gao et al., 2019; Ogawa and Rasband, 2021) and adeno-associated virus (AAV) to tag the N-terminus of Fascin1 in cultured rat hippocampal neurons. Custom single-stranded DNA oligonucleotides encoding guide RNAs (gRNAs) targeting the N-terminus (5'-TTGGCGGTCATGGTGGCGGA) of Fascin1 were synthesized, annealed, and subcloned into the pAAV-pHiUGE-smFP-V5 donor-ORF0 plasmid (Addgene #200380) after SapI restriction enzyme digestion (Ogawa et al., 2025). β-actin was endogenously tagged with EGFP using pAAV-pHITI-Actb-GFP as described (Ogawa et al., 2025) to identify and visualize sparsely distributed edited neurons for high- and super-resolution

imaging of Fascin in dendritic spines. To knockout fascin1, we employed a previously described (Ogawa et al., 2023) AAV-mediated multiplexed gRNA system. We inserted the following 3 gRNAs targeting Fascin1 into pAAV-3xgRNA-KO (Addgene #240310): TCTACCGCGATCTCGTCGGC, GCGACCTTCGCAGTCGCGAA, and GCACCCACACGGGCAAGTAC. As the control, pAAV-3xRNA-KO-template encodes three non-targeting gRNAs: CTGTCTTCATCATGGCCGAC, GTTCGCATTATCCGAACCAT, TAAGCGTCGCAAGAAGACGG. To express Cas9, we used a modified version of pAAV-pMecp2-SpCas9-spA (Addgene #60957) lacking the HA-tag. The following AAV particles were produced with the PHP.S serotype by VectorBuilder (Chicago, IL): pAAV-pHiUGE-smFP-V5-Fascin1, pAAV-pHITI-Actb-GFP, pAAV-3xgRNA-KO template, pAAV-3xgRNA-KO-Fascin1, and pAAV-pMecp2-SpCas9. For transduction of cultured neurons, we added AAV-Mecp2-SpCas9 (MOI = 50,000) together with either pHiUGE-smFP-V5-Fascin1, HITI-Actb-GFP, 3xgRNA-KO template, or 3xgRNA-KO-Fascin1 (MOI = 50,000). We applied AAV particles to DIV4 neurons for 48 hours before washout and maintained the cells until DIV21 or later for imaging and electrophysiology.

Electrophysiology

Whole-cell voltage clamp recordings were obtained from DIV21-23 rat hippocampal neurons expressing bright smFP-HA using an AxoPatch 200B amplifier (Molecular Devices), controlled by pClamp 10.1 software (Molecular Devices), low pass filtered at 5 KHz on-line and digitized at 20 KHz. Tight seals (>2 GΩ) were obtained using thin-walled boro-silicate glass microelectrodes pulled to obtain resistances between 7 and 10 MΩ. The intracellular patch solution contained the following (in mM):

potassium-gluconate 125, KCl 10, Tris-phosphocreatine 5, HEPES 10, Mg-ATP 3, Na_2-GTP 1.5, HEPES 10, $MgSO_4$ 2, $CaCl_2$ 0.1, EGTA 0.5. The pH was adjusted to 7.4 with KOH. Osmolarity was measured between 280-300 mOsm. The recording chamber was mounted on an Axiovert 100 Microscope (Karl Zeiss Microscopes) and continuously perfused (5 ml/min) with oxygenated Artificial Cerebral-Spinal Fluid (ACSF) recording solution contained the following (in mM): NaCl 126, KCl 3, NaH2PO4 1, $CaCl_2$ 2, $MgCl_2$ 1, HEPES 10 and D-glucose 25. The pH was adjusted to 7.4 with NaOH. Miniature excitatory postsynaptic currents (mEPSCs) were isolated using 1 μM TTX (R&D Systems) and 5 μM Gabazine (R&D Systems) to ACSF to block action potentials and GABAergic mPSCs, respectively. Membrane potential was held at -70 mV and recordings were performed at 27 ºC. For the chemically induced LTP, recording solution was switched to oxygenated LTP-induction solution contained (in mM): tetraethylammonium chloride (TEA-Cl) 25, $CaCl_2$ 5, $MgCl_2$ 0.1, NaCl 97, KCl 3, NaH_2PO_4 1, HEPES 10 and D-glucose 25 for 10 min. Series resistance during recordings varied from 15 to 20 MΩ and were not compensated. Recordings were terminated whenever significant increases in series resistance (> 20%) occurred. Analysis of mEPSCs was performed blind to condition with MiniAnalysis software (Synaptosoft) using a threshold of 5 pA for mEPSC amplitude. Estimation statistics were used. 5000 bootstrap samples were taken; the confidence interval was bias-corrected and accelerated. The p values reported are the likelihoods of observing the effect sizes if the null hypothesis of zero difference is true. For each permutation p value, 5000 reshuffles of the control and test labels were performed (Ho et al., 2019).

Antibodies and immunofluorescent labeling

The following antibodies were used: rabbit polyclonal anti-GFP (Invitrogen, #A11122; 1:1000), mouse monoclonal anti-α-tubulin (clone DM1A, Sigma, #MABT205; 1:1000), mouse monoclonal anti-Fascin (clone 55K2, Millipore Sigma, #MAP3582; 1:1000), rabbit monoclonal anti-Fascin (Abcam, #EP5902, KO validated; 1:500), and sheep polyclonal anti-Fascin (R&D Systems, #AF7745, KO validated; 1:1000). Mouse anti-Fascin antibody was generated using purified full-length human fascin, and recognizes fascin from mouse, rat, and human. Rabbit anti-Fascin antibody was generated using amino acids 200-400 from recombinant human Fascin and recognizes Fascin from human and mouse (predicted to recognize rat). Sheep anti-Fascin antibody was generated using full-length human Fascin1 and it detects human, rat, and mouse fascin. Triple channel immunofluorescent staining of cultured CAD cells using these three anti-fascin antibodies was found to label the same F-actin structures, with quantitative analysis showing a very high degree of colocalization as indicated by Pearson Correlation Coefficients, Manders' Colocalization Coefficients, and Costes' P-values (Supplemental figure S1 A-B).

For confocal imaging, Alexa Fluor-conjugated (AF488-, AF546-, and/or AF647) secondary antibodies raised in Donkey were diluted (1:500) in phosphate-buffered saline (PBS) containing 2% donkey serum for 1.5 hours. For STED imaging, long Stokes-shifted Abberior STAR 460L-conjugated goat anti-rabbit, STAR ORANGE-conjugated goat anti-mouse, and STAR RED-conjugated donkey anti-sheep secondary antibodies were used. Due to the cross-reactivity of goat and sheep IgGs, we employed a two-step labeling approach. Cells labeled with three primary antibodies (mouse, rabbit, and sheep) were first incubated with STAR RED-conjugated donkey anti-sheep

antibodies for 1.5 hours at room temperature, followed by three washes with PBS, PBS-0.2% Tween-20, and PBS, respectively. Cells were then incubated with both STAR 460L and STAR ORANGE-conjugated goat antibodies for 1.5 hours at room temperature, followed by three washes, and mounted in ProLong Gold antifade mount (Thermo Fisher, #P36930) for over 2 days before STED imaging.

The optimal fixation method for immunofluorescent labeling of Fascin is the use of 100% cold methanol. Briefly, cultured hippocampal neurons were rapidly fixed with 100% cold anhydrous methanol (Sigma 322415) for 10 min at -20°C, followed immediately by rehydration in PBS containing 0.1% Triton X-100, and three additional washes in PBS. Cells were blocked in PBS with 2% normal donkey serum (Sigma D9663) for 1 hour at room temperature. Neurons are incubated in a humidified chamber overnight at 4°C with primary antibodies diluted in PBS with 2% donkey serum. Cells were washed with PBS, PBS-0.05% Tween 20, and PBS, followed by incubation with the mixture of secondary antibodies for 1.5 h at room temperature. After three washes with PBS, PBS-Tween20, and PBS, the coverslips were mounted on glass slides using ProLong Gold antifade.

Microscopy and imaging

Laser scanning confocal microscopy was performed on a Nikon C2 confocal unit with four laser lines (405 nm, 488 nm, 561 nm, and 610 nm), three detectors, and either 10X/NA0.5 or 60X/NA1.4 Plan Apo objectives (Nikon Instruments Inc, Melville, New York, USA). Confocal image acquisition was done using Nikon Elements software. Stimulated Emission Depletion (STED) super-resolution imaging was performed using an Abberior Facility Line STED system (Abberior Instruments GmbH, Göttingen,

Germany) housed on an Olympus IX83 inverted microscope (Evident, Tokyo, Japan) with a 60X/NA1.4 oil immersion objective (UPLXAPO, Olympus, Japan). With the use of long Stokes-shifted Abberior STAR 460L together with STAR ORANGE and STAR Red, a single 594 nm pulsed STED depletion laser was used for simultaneous triple channel STED imaging using 485 nm, 560 nm, and 640 nm excitation lasers. Image acquisition was done using Inspector software (Abberior, Germany), and post-acquisition image enhancement and quantification were done using FIJI ImageJ software (NIH, Bethesda, MD).

Western blots

Rat hippocampal neurons were lysed directly in 1× Laemmli sample buffer at indicated timepoints, then boiled for 5 min, and vortexed for 5 min. Equal volumes of cell lysates were loaded on mini-Protean 12% Tris-glycine acrylamide gels (#4561043, Bio-Rad) and transferred to nitrocellulose. Membranes were blocked with 5% milk in PBS-Tween (0.2%) for 1 h, then incubated overnight at 4°C with rabbit anti-Neuronal Class III beta-tubulin polyclonal (#PRB-435P, Covance; 1:2000) and mouse anti-fascin (1:5000). Membranes were washed 3x in PBS-Tween then incubated in anti-rabbit-Alexa Fluor568– (Invitrogen) and anti-mouse-IRDye800-conjugated (LiCor) secondary antibodies for 1 h at room temperature. Membranes were washed 3x in PBS-Tween and then visualized using a ChemiDoc MP imaging system (Bio-Rad, Hercules, CA).

Results and discussion

Fixation methods that preserve the spatial localization of fascin

Previous studies have reported that fascin localization to F-actin bundles can be revealed with cold methanol fixation, but not aldehyde-based fixation, although the explanation for this remains unclear (Ross et al., 2000; Yamakita et al., 2011; Yamashiro et al., 1998). To systematically evaluate fixation conditions for fascin immunostaining, we examined mouse neuroblastoma CAD cells, which form prominent lamellipodia and filopodia when seeded on laminin substrates (Skruber et al., 2020; Vitriol et al., 2013). Consistent with previous findings (Hardin et al., 2025; Vignjevic et al., 2006), cold 100% methanol (-20°C) preserved fascin enrichment in F-actin-rich lamellipodia and filopodia, as evidenced by using multiple independent anti-fascin antibodies (Figure 1A, Figure S1A-C). However, cold methanol fixation disrupts the binding of phalloidin to F-actin, as reported previously (Burkel et al., 2007; Svoboda, 1992) (Figure 1A). Conversely, fixation with either 2% glutaraldehyde or 4% paraformaldehyde (PFA) resulted in robust phalloidin staining but weak or no fascin signals in actin-rich structures, essentially rendering fascin cytosolic (Figure 1A). Similarly, fixation with 50% cold methanol (Korobova and Svitkina, 2010) could not preserve the fascin localization and resulted in a substantial loss of fascin signals associated with F-actin in membrane protrusions (Figure S1D). These results demonstrate that cold 100% methanol fixation is required to accurately preserve fascin colocalization with F-actin.

Aldehyde-based cross-linking can affect antibody detection by masking specific epitopes (Metz et al., 2004; Otali et al., 2009; Scalia et al., 2017). To test whether

aldehyde-based fixation disrupts fascin antibody accessibility, we expressed exogenous GFP-fascin, and stained cells using both anti-GFP and anti-fascin antibodies. Aldehyde-based fixations, but not fixation with 100% methanol, eliminated the colocalization of GFP-fascin with F-actin bundles (Figure 1B). This was seen using both antibodies, including an anti-GFP antibody that detects GFP in PFA-fixed cells (Myers et al., 2022; Myers et al., 2020). This observation suggests that aldehyde-based fixation does not mask common epitopes on fascin. We next performed real-time imaging of GFP-fascin and mCherry-actin during the fixation process and found that GFP-fascin rapidly dissociates from F-actin upon fixation with 2% PFA, whereas most mCherry-actin signals remain (Figure 1C). Fascin is known to exhibit a dynamic and rapid binding behavior when bundling actin filaments with a kinetic off-rate of ~0.12 s^{-1} (Aratyn et al., 2007; Winkelman et al., 2016). In contrast, formaldehyde fixation is a relatively slow two-step process: an initial, rapid formation of a Schiff base (seconds), followed by a much slower crosslinking step that requires minutes or longer to form a stable bond (Hoffman et al., 2015). Given this temporal mismatch, it is highly likely that formaldehyde is incapable of crosslinking fascin to actin filaments before it dissociates. Instead, formaldehyde likely inactivates fascin molecules while they are unbound, effectively trapping them in a cytosolic state, as implied by the live imaging (Figure 1C). Together, these findings establish that rapid fixation using cold alcohol-based fixation (i.e. cold methanol or cold acetone) is required to accurately visualize fascin localization in cells, and it helps explain long-standing discrepancies in fascin localization.

Fascin is enriched in dendritic protrusions

During synaptic development, dendritic processes elaborate dendritic filopodia

that are considered as the precursor of postsynaptic dendritic spines (Lohmann and Bonhoeffer, 2008; Spence et al., 2016). A previous study using 50% methanol fixation concluded that fascin is absent from dendritic filopodia, unlike conventional filopodia and axonal growth cone filopodia (Korobova and Svitkina, 2010). Given the substantial loss of fascin associated with F-actin in lamellipodia and filopodia after 50% methanol fixation (Supplemental figure S1D), we re-examined fascin localization in dendritic compartments using cold 100% methanol fixation. Since fascin is highly enriched in axonal compartments (Hardin et al., 2025), we employed very low-density hippocampal cultures (10,000 cells/35mm dish) to examine dendritic fascin distribution and minimize interference from axonal signals. At DIV11, filopodia are the predominant type of dendritic protrusion of cultured hippocampal neurons. We observed robust enrichment of fascin in dendritic filopodia, colocalized with actin (Figure 2A, arrowheads). We also observed fascin enrichment in dendritic protrusions at DIV13 (Figure 2B). At this stage, there is a mix of dendritic filopodia (Figure 2B, arrowheads) and immature dendritic spines that are in contact with axons and exhibit slightly enlarged heads (Figure 2B, arrows). The appearance of spines becomes much more apparent in DIV18 neurons as those contacting axons exhibited clearly enlarged heads with an elevated level of fascin signals (Figure 2C, arrows). It should be noted that fascin signals are weaker in dendritic protrusions in comparison to axonal growth cones (GC, Figure 2B), but their presence in both filopodia and immature spines are clearly evident.

By DIV25, dendritic spines have become predominant in low-density hippocampal cultures where fascin can clearly be detected and appears to be enriched in spines (Figure 3A). To further confirm this observation, we examined the dendritic

localization of fascin to mature dendritic spines in high-density hippocampal cultures (250,000 cells/35mm dish). We took advantage of the sparseness of CRISPR/Cas9-based GFP- tagging of endogenous β-actin (GFP-endo-β-actin) in high-density hippocampal cultures and used GFP signals to create a mask to remove surrounding signals from neighboring non-transduced cells for better examination of fascin enrichment in mature dendritic spines. Consistent with our observation in low density hippocampal cultures, we found that fascin is enriched in mature dendritic spines in high-density hippocampal cultures (Figure 3B). Quantitative analysis of the spine-to-shaft ratio confirmed elevated levels of fascin in spines relative to the neighboring dendritic shaft in both the low-density and high-density hippocampal cultures (Figure 3C). Together, our data demonstrates that fascin is not only present in dendritic compartments but also enriched in dendritic protrusions of filopodia and spines, suggesting a potential role for fascin in postsynaptic function.

Fascin in spines forms nanoscale foci

To further investigate the spine localization of fascin molecules, we utilized CRISPR-based gene editing to fluorescently tag endogenous fascin1 at its N-terminus with spaghetti monster fluorescent protein with V5 epitopes (smFP-V5). Consistent with our immunostaining data, smFP-V5-endo-fascin1 signals are enriched in dendritic spines, as well as in the growth cone with filopodia (Figure 4A). Interestingly, smFP-V5-endo-fascin1 signals appear to be mostly enriched in the spine heads and exhibit a punctate pattern (Figure 4A, yellow arrows), suggesting a potential sub-spine organization of fascin. To investigate the nanoscale distribution of fascin in spines, we next performed super-resolution STED imaging. High-density hippocampal cultures

were infected with AAVs at DIV4 to tag endogenous β-actin with GFP, fixed with cold 100% methanol at DIV25, and triple-labeled for GFP (for GFP-endo-β-actin), bassoon (for presynaptic active zones), and fascin. While fascin signals are clearly enriched in actin-rich dendritic spines under confocal microscopy, STED imaging reveals that fascin is distributed as discrete foci throughout the actin-rich spine head, but rarely in the spine neck (Figure 4B-C, Figure S2A). Quantification of individual fascin foci in spines finds that they range in size from 40 nm to 160 nm, with an average of 97 nm (Figure 4D). This punctate pattern of fascin signals in spines contrasts sharply with the continuous fascin distribution observed in lamellipodia and axonal growth cones (Figure S2B-C), indicating that these nanoscale foci are unlikely a result of fixation or immunolabeling artifacts. The nanoscale organization of fascin in dendritic spines is consistent with the lack of tight F-actin bundles in dendritic spines, suggesting a potentially novel function for fascin in regulating dendritic F-actin networks.

Fascin is essential for synaptic plasticity

To test the function of fascin in dendritic spines, we utilized AAV-based CRISPR/Cas9-mediated knockout (KO) of fascin1 in cultured hippocampal neurons. Cells were infected at DIV4 with AAV expressing spCas9, together with AAV expressing either smFP-HA (3xgRNA-KO template, expressing three non-targeting gRNAs) or smFP-HA plus three gRNAs targeting the coding region of FSCN1 (3xgRNA-KO-Fascin1). Fascin was effectively knocked out using this approach, as demonstrated by both immunostaining and western blotting (Figure S3A-D). At DIV25, HA-positive neurons (indicating gRNA-expressing cells) displayed essentially no fascin fluorescence (Figure S3A). Western blotting revealed the relatively late onset of fascin KO (~12 days

post infection) in cultured hippocampal neurons, with the remaining fascin levels likely representing a small pool of non-HA-expressing cells (Figure S3C-D). This delayed timeline is consistent with a recent report showing continued editing of post-mitotic cells for at least 16 days after viral sgRNA and Cas9 infection (Ramadoss et al., 2025). We also found that fascin expression gradually increases over the first three weeks of development in culture (Figure S3E), consistent with previous reports (De Arcangelis et al., 2004; Zhang et al., 2008).

Due to the late onset of CRISPR-based fascin KO (~DIV16, see Figure S3C-D) relative to neuronal development, we anticipated that the dendritic and synaptic development of hippocampal neurons in culture would not be affected. Indeed, we found that fascin KO did not significantly affect dendritic spine density or morphology, as compared to control neurons (Figure 5A-D). Consistently, whole-cell patch-clamp recordings revealed no difference in the frequency or amplitude of miniature excitatory postsynaptic currents (mEPSCs) between control (3xgRNA-KO template) and KO (3xgRNA-KO-Fascin1) cells (Figure 5E-G). To test whether fascin is required for synaptic plasticity, we used a well-established chemical LTP (cLTP) protocol in which Tetraethylammonium (TEA) is applied to block potassium channels (Gu et al., 2010; Hille, 1967; Huang and Malenka, 1993). Consistent with previous findings, brief exposure to 25 mM TEA produced robust potentiation of mEPSC frequency and amplitude in control neurons (Figure 5E-F, 5H). In contrast, fascin KO neurons showed no increase in mEPSC frequency or amplitude (Figure 5E-F, 5I). These results identify fascin as a key actin regulator for activity-dependent synaptic remodeling.

The actin cytoskeleton is highly enriched in postsynaptic spines where it not only

supports the distinct spine shapes but also provides a scaffold for the spatiotemporal organization of postsynaptic receptors and signaling components (MacGillavry et al., 2013; Okabe, 2020). Importantly, postsynaptic remodeling during learning and memory depends on highly regulated actin dynamics, and its disruption is strongly associated with neurological conditions (Bosch and Hayashi, 2012; Cingolani and Goda, 2008; Hotulainen and Hoogenraad, 2010). While tremendous progress has been made in our understanding of actin-based cellular activities, we still lack a detailed picture of its unique organization and dynamic regulation in synaptic compartments. In this study, we establish fascin as a key actin regulator of postsynaptic structure and function, revising the prevailing view that fascin is neither present nor functionally relevant in dendritic compartments. These findings are consistent with recent studies that identify fascin1 as a target for spine formation and memory consolidation (Shivkumar et al., 2025; Yang et al., 2025).

At this moment, how fascin regulates the spine F-actin network remains unknown. Given the lack of tight actin bundles in the spine neck, it is plausible that fascin adopts a distinct organization within the mostly branched F-actin networks in spine heads to function in a complementary, but non-overlapping, manner from other actin bundling proteins in spines (Chazeau and Giannone, 2016; Winkelman et al., 2016). For example, α-actinin-mediated crosslinking of actin filaments has been shown to be important for proper spine development and maintenance, as well as for linking actin to the postsynaptic density (Hlushchenko et al., 2018; Wyszynski et al., 1997). However, unlike α-actinin, which localizes throughout dendritic spines (Hodges et al., 2014; Wyszynski et al., 1998), the appearance of fascin in discrete nanoscale foci

specifically within spine heads (Figure 4B) indicates a potential role in the fine-tuning of actin dynamics within its densely branched network. Recent evidence in non-neuronal contexts also support a role for fascin in the regulation of branched actin networks (Chikireddy et al., 2024; Wubshet et al., 2021). Future studies are clearly needed to elucidate how fascin engages with F-actin in postsynaptic compartments.

Figure Legends

Figure 1. Methanol fixation is required to capture the cellular localization of fascin. (**A**) Representative immunofluorescent images of CAD cells fixed with 100% cold methanol (top row), 2% glutaraldehyde (middle row), or 4% PFA (bottom row). Cells were stained with mouse (M) anti-fascin, rabbit (R) anti-fascin, and phalloidin-AlexaFluor546. Regions enclosed by dashed rectangles are shown at a higher magnification on the right, highlighting the actin-rich lamellipodia and filopodia. Arrows highlight weak fascin signals remaining after aldehyde fixation. (**B**) Representative images of CAD cells expressing GFP-fascin for approximately 24 hours and fixed with either 100% cold methanol (left panels) or 4% PFA (right panels). Cells were stained with mouse (M) anti-Fascin and rabbit anti-GFP. (**C**) Sequential images showing live CAD cells co-expressing GFP-fascin and mCherry-γ-actin, before and after fixation with 2% PFA (added at 0" seconds). Time shown in seconds (total duration 70 seconds). Scale bars: 10 μm.

Figure 2. Fascin localizes to dendritic filopodia and immature spine-like protrusions during neuronal development. (**A**) Representative images of low-density cultured hippocampal neurons at DIV11 fixed with 100% cold methanol and labelled for endogenous fascin (cyan) and actin (magenta). Inset in right panel is a linescan showing correlation of fascin and actin levels across multiple filopodia from highlighted region. Arrowheads highlight filopodia with high fascin enrichment. Scale bar = 10 μm. (**B**) Representative images of low-density cultured hippocampal neurons at DIV13 neurons fixed and stained as above. Arrows highlight nascent spines with slightly enlarged heads and fascin enrichment that are in contact with axons. GC: axonal

growth cone. Scale bar = 10 μm. (**C**) Representative images of DIV18 neurons fixed and stained as above. Panels on right represent high magnification of corresponding boxed regions from left. Arrows highlight spines with enlarged heads, and arrowheads highlight filopodia. Left scale bar = 10 μm, right scale bars = 2 μm.

Figure 3. Fascin is enriched in mature dendritic spines. (**A**) Representative images of low-density cultured hippocampal neurons at DIV28 fixed with 100% cold methanol and labelled for endogenous fascin (cyan) and actin (magenta). Left scale bar = 10 μm, right scale bar = 5 μm. (**B**) Representative image of a neuron from high-density hippocampal culture expressing GFP-tagged endogenous β-actin, fixed with 100% cold methanol at DIV28, and labelled for fascin (cyan) and GFP (magenta). GFP-β-actin signal was used as mask to isolate individual neuron from neighboring cells. Right, high magnification panels of boxed regions from image on left. Left scale bar = 10 μm, right scale bars = 2 μm. (**C**) Quantification of fascin enrichment in dendritic spines. Graphs show the ratio of fascin or β-actin fluorescence intensity in spine heads compared to the intensity of an equal-sized area of the neighboring dendritic shaft. *n* = fields of view, representing >200 spines from low density cultures and >500 spines from high density cultures, from 3 independent cultures. Error bars represent SEM.

Figure 4. Fascin is enriched in dendritic spine heads as discrete nanoscale foci. (**A**) Representative images of hippocampal neurons at DIV21 with endogenous fascin1 tagged by CRISPR-mediated knock-in of smFP-V5 (cyan). The left panel shows a portion of the dendritic arbor of a neuron expressing smFP-V5-fascin1 (cyan) among the high-density hippocampal culture (immunofluorescently labeled for actin, magenta). Fascin signals are present in dendritic arbors and enriched in dendritic spines, as well

as an axonal growth cone (GC). The regions enclosed by dashed rectangles are shown in a high magnification on the right, in which fascin signals are represented using a cyan hot look-up table. Yellow arrows indicate spines with punctate fascin distribution within the spine heads, whereas white arrows indicate small spines with fascin in their heads. Left scale bar = 10 μm, right scale bars = 2 μm. (**B**) Representative confocal (top row) and STED (bottom row) images of high-density hippocampal cultures expressing GFP-tagged endogenous β-actin, fixed at DIV25 with 100% cold methanol, and triple stained for fascin (cyan), β-actin (magenta), and bassoon (yellow). GFP-β-actin signal was used as mask to isolate individual neurons from neighboring cells. Fascin appears as discrete foci within actin-rich spine heads (arrows), but not in spine necks. A portion of the dendrite (dashed rectangle) is shown on the right, in a higher magnification with three channels merged. Scale bars = 1 μm. (**C**) High magnification images of individual spines in (B) showing punctate fascin distribution (spines outlined in blue). Scale bar = 1 μm. (**D**) Histogram showing width of individual fascin foci in spine heads, assigned within 20 nm bins. Gray bar shows accumulated frequency of foci width. A total of 6 STED images and more than 30 spines were analyzed.

Figure 5. Fascin is required for synaptic potentiation in mature hippocampal neurons. (**A**) Representative images of dendritic spines from control (3xgRNA-KO template) or fascin KO (3xgRNA-KO-Fascin1) high-density hippocampal neurons at DIV25-28. Co-expressed smFP is used to visualize spine morphology. Scale bar = 5 μm. (**B-D**) Plots show no differences in spine density, length, or width between control and fascin KO cells under basal conditions (not significant by unpaired student's *t*-test). Error bars are ± SEM. (**E**) Representative sample traces of mEPSCs from whole-cell

patch-clamp recordings of control and fascin KO before and after application of 25 mM TEA. (**F**) Average mEPSC waveforms before (black) and after (gray) TEA application in control (top) and fascin1 KO (bottom) neurons. (**G-I**) Gardner-Altman estimation plots showing that the differences in mEPSC amplitude (top) and amplitude (bottom) between the control (N=23) and fascin KO (N=15) groups. (G) The baseline synaptic transmission was not affected by fascin KO, as the unpaired mean differences for the frequency and amplitude are 0.387 Hz (95% confidence interval (CI), -0.13, 1.15) and 0.694 pA (95% CI, -1.25, 2.77). P values of the two-sided permutation *t*-test on the frequency and amplitude are 0.25 and 0.52, respectively. (H) TEA-cLTP significantly increased the frequency and amplitude of synaptic transmission in the control group. The unpaired mean differences before and after TEA treatment are 1.06 Hz (95% CI, 0.503, 1.6) and 2.55 pA (95% CI, 0.639, 4.61). P values of the two-sided permutation *t*-test are 0.0006 and 0.03, respectively. (I) TEA-cLTP did not increase, but decreased, the frequency and amplitude of synaptic transmission in the fascin KO group. The unpaired mean differences before and after TEA treatment are -0.935 Hz (95% CI, -1.59, -0.466) and -2.08 pA (95% CI, -3.96, -0.478). P values of the two-sided permutation *t*-test are 0.04 and 0.0004, respectively.

Supplemental Figures

Figure S1. Fascin localization after methanol fixation is detected with multiple antibodies. (A) Representative images of CAD cells fixed with 100% cold methanol (−20 °C) and stained with three independent anti-fascin antibodies (raised in mouse (M), rabbit (R), and sheep(S)). (B) Left, magnified image from the boxed region of (A), showing essentially the same fascin enrichment pattern in lamellipodia and filopodia using three independent antibodies. Right, fluorescence intensity profiles corresponding to the dotted white line from image on the left. (C) Quantification of colocalization, analyzed for each pairing of anti-fascin antibodies. (D) Fixation with 50% methanol compromises fascin labeling, compared to fixation with 100% methanol. Representative images of CAD cells fixed with either 100% or 50% cold methanol (−20 °C) and stained with mouse (M) anti-fascin and rabbit (R) anti-fascin antibodies.

Figure S2. STED imaging of fascin. (A) Representative confocal image of a DIV25 hippocampal neuron expressing GFP-tagged endogenous β-actin, fixed with 100% cold methanol, and labeled with mouse anti-Bassoon, rabbit anti-GFP, and sheep anti-fascin antibodies. Right, STED images of boxed regions from merged image on left, showing fascin foci in dendritic spine heads. (B) Representative confocal and STED images of CAD cell lamellipodia, labelled for endogenous fascin (cyan) and actin (magenta), showing continuous fascin staining pattern along F-actin bundles. (C) Representative STED images of growth cones from primary hippocampal neurons, labelled for endogenous fascin (cyan) and actin (magenta), showing continuous fascin staining pattern along F-actin bundles.

Figure S3. Fascin1 KO validation in hippocampal neurons. (A) Representative immunofluorescence images of methanol-fixed DIV25 hippocampal neurons that were infected on DIV5 with AAV to express Cas9 and either control (3xgRNA-KO template) or fascin KO (3xgRNA-KO-Fascin1), both of which co-express smFP-HA. Methanol-fixed cells were immunostained for HA to identify transduced cells (magenta) and evaluate fascin levels (cyan). Fascin immunoreactivity is absent in HA-positive fascin KO neurons. (B) Violin and box plot showing the loss of fascin fluorescence intensity in KO cells relative to control neurons. N = number of cells analyzed from 3 separate cultures. (C) Representative western blots showing the levels of fascin and tubulin (used as a loading control) at various times post AAV infection (i.e. DIV 5). (D) Analysis of western blots, showing the effective KO of fascin 12 days post-AAV infection. For each timepoint, samples were normalized to tubulin loading control, and fascin levels in control and KO cells were presented relative to eGFP-expressing neurons. n = 3 separate neuronal cultures. (E) Quantification of fascin levels during primary neuron development. Fascin levels were normalized to tubulin and presented relative to the initial DIV6 timepoint. Error bars are ± SEM.

References

Adams, J.C. 2004. Roles of fascin in cell adhesion and motility. *Curr Opin Cell Biol*. 16:590-596.

Anggono, V., and R.L. Huganir. 2012. Regulation of AMPA receptor trafficking and synaptic plasticity. *Curr Opin Neurobiol*. 22:461-469.

Aratyn, Y.S., T.E. Schaus, E.W. Taylor, and G.G. Borisy. 2007. Intrinsic dynamic behavior of fascin in filopodia. *Mol Biol Cell*. 18:3928-3940.

Benke, T., and S.F. Traynelis. 2019. AMPA-Type Glutamate Receptor Conductance Changes and Plasticity: Still a Lot of Noise. *Neurochemical research*. 44:539-548.

Bin Ibrahim, M.Z., A. Benoy, and S. Sajikumar. 2022. Long-term plasticity in the hippocampus: maintaining within and 'tagging' between synapses. *The FEBS journal*. 289:2176-2201.

Bosch, M., J. Castro, T. Saneyoshi, H. Matsuno, M. Sur, and Y. Hayashi. 2014. Structural and molecular remodeling of dendritic spine substructures during long-term potentiation. *Neuron*. 82:444-459.

Bosch, M., and Y. Hayashi. 2012. Structural plasticity of dendritic spines. *Current opinion in neurobiology*. 22:383-388.

Bucher, M., T. Fanutza, and M. Mikhaylova. 2020. Cytoskeletal makeup of the synapse: Shaft versus spine. *Cytoskeleton (Hoboken)*. 77:55-64.

Burkel, B.M., G. von Dassow, and W.M. Bement. 2007. Versatile fluorescent probes for actin filaments based on the actin-binding domain of utrophin. *Cell Motil Cytoskeleton*. 64:822-832.

Chazeau, A., and G. Giannone. 2016. Organization and dynamics of the actin cytoskeleton during dendritic spine morphological remodeling. *Cellular and molecular life sciences : CMLS*. 73:3053-3073.

Chhabra, E.S., and H.N. Higgs. 2007. The many faces of actin: matching assembly factors with cellular structures. *Nat Cell Biol*. 9:1110-1121.

Chidambaram, S.B., A.G. Rathipriya, S.R. Bolla, A. Bhat, B. Ray, A.M. Mahalakshmi, T. Manivasagam, A.J. Thenmozhi, M.M. Essa, G.J. Guillemin, R. Chandra, and M.K. Sakharkar. 2019. Dendritic spines: Revisiting the physiological role. *Progress in neuro-psychopharmacology & biological psychiatry*. 92:161-193.

Chikireddy, J., L. Lengagne, R. Le Borgne, C. Durieu, H. Wioland, G. Romet-Lemonne, and A. Jégou. 2024. Fascin-induced bundling protects actin filaments from disassembly by cofilin. *J Cell Biol*. 223.

Cingolani, L.A., and Y. Goda. 2008. Actin in action: the interplay between the actin cytoskeleton and synaptic efficacy. *Nat Rev Neurosci*. 9:344-356.

Citri, A., and R.C. Malenka. 2008. Synaptic plasticity: multiple forms, functions, and mechanisms. *Neuropsychopharmacology : official publication of the American College of Neuropsychopharmacology*. 33:18-41.

Cohan, C.S., E.A. Welnhofer, L. Zhao, F. Matsumura, and S. Yamashiro. 2001. Role of the actin bundling protein fascin in growth cone morphogenesis: localization in filopodia and lamellipodia. *Cell Motil Cytoskeleton*. 48:109-120.

De Arcangelis, A., E. Georges-Labouesse, and J.C. Adams. 2004. Expression of fascin-1, the gene encoding the actin-bundling protein fascin-1, during mouse embryogenesis. *Gene Expr Patterns*. 4:637-643.

Gao, Y., E. Hisey, T.W.A. Bradshaw, E. Erata, W.E. Brown, J.L. Courtland, A. Uezu, Y. Xiang, Y. Diao, and S.H. Soderling. 2019. Plug-and-Play Protein Modification Using Homology-Independent Universal Genome Engineering. *Neuron*. 103:583-597.e588.

Ge, Y., Z. Dong, R.C. Bagot, J.G. Howland, A.G. Phillips, T.P. Wong, and Y.T. Wang. 2010. Hippocampal long-term depression is required for the consolidation of spatial memory. *Proc Natl Acad Sci U S A*. 107:16697-16702.

Gu, J., C.W. Lee, Y. Fan, D. Komlos, X. Tang, C. Sun, K. Yu, H.C. Hartzell, G. Chen, J.R. Bamburg, and J.Q. Zheng. 2010. ADF/cofilin-mediated actin dynamics regulate AMPA receptor trafficking during synaptic plasticity. *Nat Neurosci*. 13:1208-1215.

Hardin, K.R., A.B. Penas, S. Joubert, C. Ye, K.R. Myers, and J.Q. Zheng. 2025. A critical role for the Fascin family of actin bundling proteins in axon development, brain wiring and function. *Mol Cell Neurosci*:104027.

Hille, B. 1967. The selective inhibition of delayed potassium currents in nerve by tetraethylammonium ion. *J Gen Physiol*. 50:1287-1302.

Hlushchenko, I., P. Khanal, A. Abouelezz, V.O. Paavilainen, and P. Hotulainen. 2018. ASD-Associated De Novo Mutations in Five Actin Regulators Show Both Shared and Distinct Defects in Dendritic Spines and Inhibitory Synapses in Cultured Hippocampal Neurons. *Front Cell Neurosci*. 12:217.

Ho, J., T. Tumkaya, S. Aryal, H. Choi, and A. Claridge-Chang. 2019. Moving beyond P values: data analysis with estimation graphics. *Nat Methods*. 16:565-566.

Hodges, J.L., S.M. Vilchez, H. Asmussen, L.A. Whitmore, and A.R. Horwitz. 2014. α-Actinin-2 mediates spine morphology and assembly of the post-synaptic density in hippocampal neurons. *PLoS One*. 9:e101770.

Hoffman, E.A., B.L. Frey, L.M. Smith, and D.T. Auble. 2015. Formaldehyde crosslinking: a tool for the study of chromatin complexes. *J Biol Chem*. 290:26404-26411.

Hotulainen, P., and C.C. Hoogenraad. 2010. Actin in dendritic spines: connecting dynamics to function. *J Cell Biol*. 189:619-629.

Hotulainen, P., O. Llano, S. Smirnov, K. Tanhuanpaa, J. Faix, C. Rivera, and P. Lappalainen. 2009. Defining mechanisms of actin polymerization and depolymerization during dendritic spine morphogenesis. *J Cell Biol*. 185:323-339.

Huang, Y.Y., and R.C. Malenka. 1993. Examination of TEA-induced synaptic enhancement in area CA1 of the hippocampus: the role of voltage-dependent Ca2+ channels in the induction of LTP. *J Neurosci*. 13:568-576.

Jansen, S., A. Collins, C. Yang, G. Rebowski, T. Svitkina, and R. Dominguez. 2011. Mechanism of actin filament bundling by fascin. *J Biol Chem*. 286:30087-30096.

Korobova, F., and T. Svitkina. 2010. Molecular architecture of synaptic actin cytoskeleton in hippocampal neurons reveals a mechanism of dendritic spine morphogenesis. *Mol Biol Cell*. 21:165-176.

Krey, J.F., E.S. Krystofiak, R.A. Dumont, S. Vijayakumar, D. Choi, F. Rivero, B. Kachar, S.M. Jones, and P.G. Barr-Gillespie. 2016. Plastin 1 widens stereocilia by transforming actin filament packing from hexagonal to liquid. *J Cell Biol*. 215:467-482.

Lei, W., O.F. Omotade, K.R. Myers, and J.Q. Zheng. 2016. Actin cytoskeleton in dendritic spine development and plasticity. *Curr Opin Neurobiol*. 39:86-92.

Li, A., J.C. Dawson, M. Forero-Vargas, H.J. Spence, X. Yu, I. König, K. Anderson, and L.M. Machesky. 2010. The actin-bundling protein fascin stabilizes actin in invadopodia and potentiates protrusive invasion. *Curr Biol*. 20:339-345.

Lima Caldeira, G., J. Peça, and A.L. Carvalho. 2019. New insights on synaptic dysfunction in neuropsychiatric disorders. *Current opinion in neurobiology*. 57:62-70.

Lohmann, C., and T. Bonhoeffer. 2008. A role for local calcium signaling in rapid synaptic partner selection by dendritic filopodia. *Neuron*. 59:253-260.

Lu, Z., M. Piechowicz, and S. Qiu. 2016. A Simplified Method for Ultra-Low Density, Long-Term Primary Hippocampal Neuron Culture. *Journal of visualized experiments : JoVE*.

MacGillavry, H.D., Y. Song, S. Raghavachari, and T.A. Blanpied. 2013. Nanoscale scaffolding domains within the postsynaptic density concentrate synaptic AMPA receptors. *Neuron*. 78:615-622.

Malenka, R.C. 1994. Synaptic plasticity in the hippocampus: LTP and LTD. *Cell*. 78:535-538.

Martin, S.J., P.D. Grimwood, and R.G. Morris. 2000. Synaptic plasticity and memory: an evaluation of the hypothesis. *Annual review of neuroscience*. 23:649-711.

Metz, B., G.F. Kersten, P. Hoogerhout, H.F. Brugghe, H.A. Timmermans, A. de Jong, H. Meiring, J. ten Hove, W.E. Hennink, D.J. Crommelin, and W. Jiskoot. 2004. Identification of formaldehyde-induced modifications in proteins: reactions with model peptides. *The Journal of biological chemistry*. 279:6235-6243.

Monday, H.R., and P.E. Castillo. 2017. Closing the gap: long-term presynaptic plasticity in brain function and disease. *Current opinion in neurobiology*. 45:106-112.

Myers, K.R., Y. Fan, P. McConnell, J.A. Cooper, and J.Q. Zheng. 2022. Actin capping protein regulates postsynaptic spine development through CPI-motif interactions. *Front Mol Neurosci*. 15:1020949.

Myers, K.R., K. Yu, J. Kremerskothen, E. Butt, and J.Q. Zheng. 2020. The Nebulin Family LIM and SH3 Proteins Regulate Postsynaptic Development and Function. *J Neurosci*. 40:526-541.

Nimchinsky, E.A., B.L. Sabatini, and K. Svoboda. 2002. Structure and function of dendritic spines. *Annu Rev Physiol*. 64:313-353.

Nishiyama, J. 2019. Plasticity of dendritic spines: Molecular function and dysfunction in neurodevelopmental disorders. *Psychiatry and clinical neurosciences*. 73:541-550.

Ogawa, Y., B.C. Lim, S. George, J.A. Oses-Prieto, J.M. Rasband, Y. Eshed-Eisenbach, H. Hamdan, S. Nair, F. Boato, E. Peles, A.L. Burlingame, L. Van Aelst, and M.N. Rasband. 2023. Antibody-directed extracellular proximity biotinylation reveals that Contactin-1 regulates axo-axonic innervation of axon initial segments. *Nat Commun*. 14:6797.

Ogawa, Y., D.V.M. Nguyen, A. Ogawa, and M.N. Rasband. 2025. Hide-and-Seek genome editing reveals that Gephyrin is required for axo-axonic synapse assembly. *Proc Natl Acad Sci U S A*. 122:e2500726122.

Ogawa, Y., and M.N. Rasband. 2021. Endogenously expressed Ranbp2 is not at the axon initial segment. *Journal of cell science*. 134.

Okabe, S. 2020. Regulation of actin dynamics in dendritic spines: Nanostructure, molecular mobility, and signaling mechanisms. *Mol Cell Neurosci*. 109:103564.

Otali, D., C.R. Stockard, D.K. Oelschlager, W. Wan, U. Manne, S.A. Watts, and W.E. Grizzle. 2009. Combined effects of formalin fixation and tissue processing on immunorecognition. *Biotech Histochem*. 84:223-247.

Parker, S.S., K.T. Ly, A.D. Grant, J. Sweetland, A.M. Wang, J.D. Parker, M.R. Roman, K. Saboda, D.J. Roe, M. Padi, C.W. Wolgemuth, P. Langlais, and G. Mouneimne. 2023. EVL and MIM/MTSS1 regulate actin cytoskeletal remodeling to promote dendritic filopodia in neurons. *J Cell Biol*. 222.

Pollard, T.D., L. Blanchoin, and R.D. Mullins. 2000. Molecular mechanisms controlling actin filament dynamics in nonmuscle cells. *Annu Rev Biophys Biomol Struct*. 29:545-576.

Pollard, T.D., and G.G. Borisy. 2003. Cellular motility driven by assembly and disassembly of actin filaments. *Cell*. 112:453-465.

Pollitt, S.L., K.R. Myers, J. Yoo, and J.Q. Zheng. 2020. LIM and SH3 protein 1 localizes to the leading edge of protruding lamellipodia and regulates axon development. *Mol Biol Cell*. 31:2718-2732.

Qi, Y., J.K. Wang, M. McMillian, and D.M. Chikaraishi. 1997. Characterization of a CNS cell line, CAD, in which morphological differentiation is initiated by serum deprivation. *J Neurosci*. 17:1217-1225.

Ramadoss, G.N., S.J. Namaganda, J.R. Hamilton, R. Sharma, K.G. Chow, B.L. Macklin, M. Sun, J.C. Liu, C. Fellmann, H.L. Watry, J. Jin, B.S. Perez, C.R.S. Espinoza, M.P. Matia, S.H. Lu, L.M. Judge, A. Nussenzweig, B. Adamson, N. Murthy, J.A. Doudna, M. Kampmann, and B.R. Conklin. 2025. Neuronal DNA repair reveals strategies to influence CRISPR editing outcomes. *bioRxiv*.

Revenu, C., R. Athman, S. Robine, and D. Louvard. 2004. The co-workers of actin filaments: from cell structures to signals. *Nature reviews. Molecular cell biology*. 5:635-646.

Ross, R., H. Jonuleit, M. Bros, X.L. Ross, S. Yamashiro, F. Matsumura, A.H. Enk, J. Knop, and A.B. Reske-Kunz. 2000. Expression of the actin-bundling protein fascin in cultured human dendritic cells correlates with dendritic morphology and cell differentiation. *J Invest Dermatol*. 115:658-663.

Sasaki, Y., K. Hayashi, T. Shirao, R. Ishikawa, and K. Kohama. 1996. Inhibition by drebrin of the actin-bundling activity of brain fascin, a protein localized in filopodia of growth cones. *J Neurochem*. 66:980-988.

Scalia, C.R., G. Boi, M.M. Bolognesi, L. Riva, M. Manzoni, L. DeSmedt, F.M. Bosisio, S. Ronchi, B.E. Leone, and G. Cattoretti. 2017. Antigen Masking During Fixation and Embedding, Dissected. *J Histochem Cytochem*. 65:5-20.

Shivkumar, A., K.R. Berg, K.C. Sibucao, G. Leriche, L.E. Dozier, C.A. Espinoza, G.N. Patrick, Z. Gaieb, C. Seitz, R.E. Amaro, H.H. Park, H.S. Hoe, J. Wozniak, D.J. Gonzalez, S. Sinha, P. Ghosh, and J. Yang. 2025. Nootropic benzothiazoles promote dendritic spine formation by targeting fascin-1. *J Biol Chem*. 301:110572.

Skruber, K., P.V. Warp, R. Shklyarov, J.D. Thomas, M.S. Swanson, J.L. Henty-Ridilla, T.A. Read, and E.A. Vitriol. 2020. Arp2/3 and Mena/VASP Require Profilin 1 for Actin Network Assembly at the Leading Edge. *Curr Biol*. 30:2651-2664.e2655.

Spence, E.F., D.J. Kanak, B.R. Carlson, and S.H. Soderling. 2016. The Arp2/3 Complex Is Essential for Distinct Stages of Spine Synapse Maturation, Including Synapse Unsilencing. *J Neurosci*. 36:9696-9709.

Stefen, H., C. Chaichim, J. Power, and T. Fath. 2016. Regulation of the Postsynaptic Compartment of Excitatory Synapses by the Actin Cytoskeleton in Health and Its Disruption in Disease. *Neural Plast*. 2016:2371970.

Svoboda, K.K. 1992. Embryonic corneal epithelial actin alters distribution in response to laminin. *Invest Ophthalmol Vis Sci*. 33:324-333.

Takeuchi, T., A.J. Duszkiewicz, and R.G. Morris. 2014. The synaptic plasticity and memory hypothesis: encoding, storage and persistence. *Philosophical transactions of the Royal Society of London. Series B, Biological sciences*. 369:20130288.

Vignjevic, D., S. Kojima, Y. Aratyn, O. Danciu, T. Svitkina, and G.G. Borisy. 2006. Role of fascin in filopodial protrusion. *J Cell Biol*. 174:863-875.

Vitriol, E.A., L.M. McMillen, M. Kapustina, S.M. Gomez, D. Vavylonis, and J.Q. Zheng. 2015. Two functionally distinct sources of actin monomers supply the leading edge of lamellipodia. *Cell Rep*. 11:433-445.

Vitriol, E.A., A.L. Wise, M.E. Berginski, J.R. Bamburg, and J.Q. Zheng. 2013. Instantaneous inactivation of cofilin reveals its function of F-actin disassembly in lamellipodia. *Molecular Biology of the Cell*. 24:2238-2247.

Walker, C.K., and J.H. Herskowitz. 2021. Dendritic Spines: Mediators of Cognitive Resilience in Aging and Alzheimer's Disease. *The Neuroscientist : a review journal bringing neurobiology, neurology and psychiatry*. 27:487-505.

Winkelman, J.D., C. Suarez, G.M. Hocky, A.J. Harker, A.N. Morganthaler, J.R. Christensen, G.A. Voth, J.R. Bartles, and D.R. Kovar. 2016. Fascin- and α-Actinin-Bundled Networks Contain Intrinsic Structural Features that Drive Protein Sorting. *Curr Biol*. 26:2697-2706.

Wubshet, N.H., Y. Bashirzadeh, and A.P. Liu. 2021. Fascin-induced actin protrusions are suppressed by dendritic networks in giant unilamellar vesicles. *Mol Biol Cell*. 32:1634-1640.

Wyszynski, M., V. Kharazia, R. Shanghvi, A. Rao, A.H. Beggs, A.M. Craig, R. Weinberg, and M. Sheng. 1998. Differential Regional Expression and Ultrastructural Localization of α-Actinin-2, a Putative NMDA Receptor-Anchoring Protein, in Rat Brain. *The Journal of Neuroscience*. 18:1383-1392.

Wyszynski, M., J. Lin, A. Rao, E. Nigh, A.H. Beggs, A.M. Craig, and M. Sheng. 1997. Competitive binding of alpha-actinin and calmodulin to the NMDA receptor. *Nature*. 385:439-442.

Yamakita, Y., F. Matsumura, M.W. Lipscomb, P.C. Chou, G. Werlen, J.K. Burkhardt, and S. Yamashiro. 2011. Fascin1 promotes cell migration of mature dendritic cells. *J Immunol*. 186:2850-2859.

Yamashiro, S., Y. Yamakita, S. Ono, and F. Matsumura. 1998. Fascin, an actin-bundling protein, induces membrane protrusions and increases cell motility of epithelial cells. *Mol Biol Cell*. 9:993-1006.

Yang, Z.J., D.Y. Yu, F.F. Gao, D.Y. Zhou, Y.N. Wu, X.X. Yang, J. Chen, J.S. Yang, M.Q. Shen, Y.X. Zhang, L. Wei, and C.X. Yan. 2025. The Histone Lysine Demethylase KDM7A Contributes to Reward Memory via Fscn1-Induced Synaptic Plasticity in the Medial Prefrontal Cortex. *Adv Sci (Weinh)*. 12:e2405352.

Zhang, F.R., L.H. Tao, Z.Y. Shen, Z. Lv, L.Y. Xu, and E.M. Li. 2008. Fascin expression in human embryonic, fetal, and normal adult tissue. *J Histochem Cytochem*. 56:193-199.

Figures 1-5

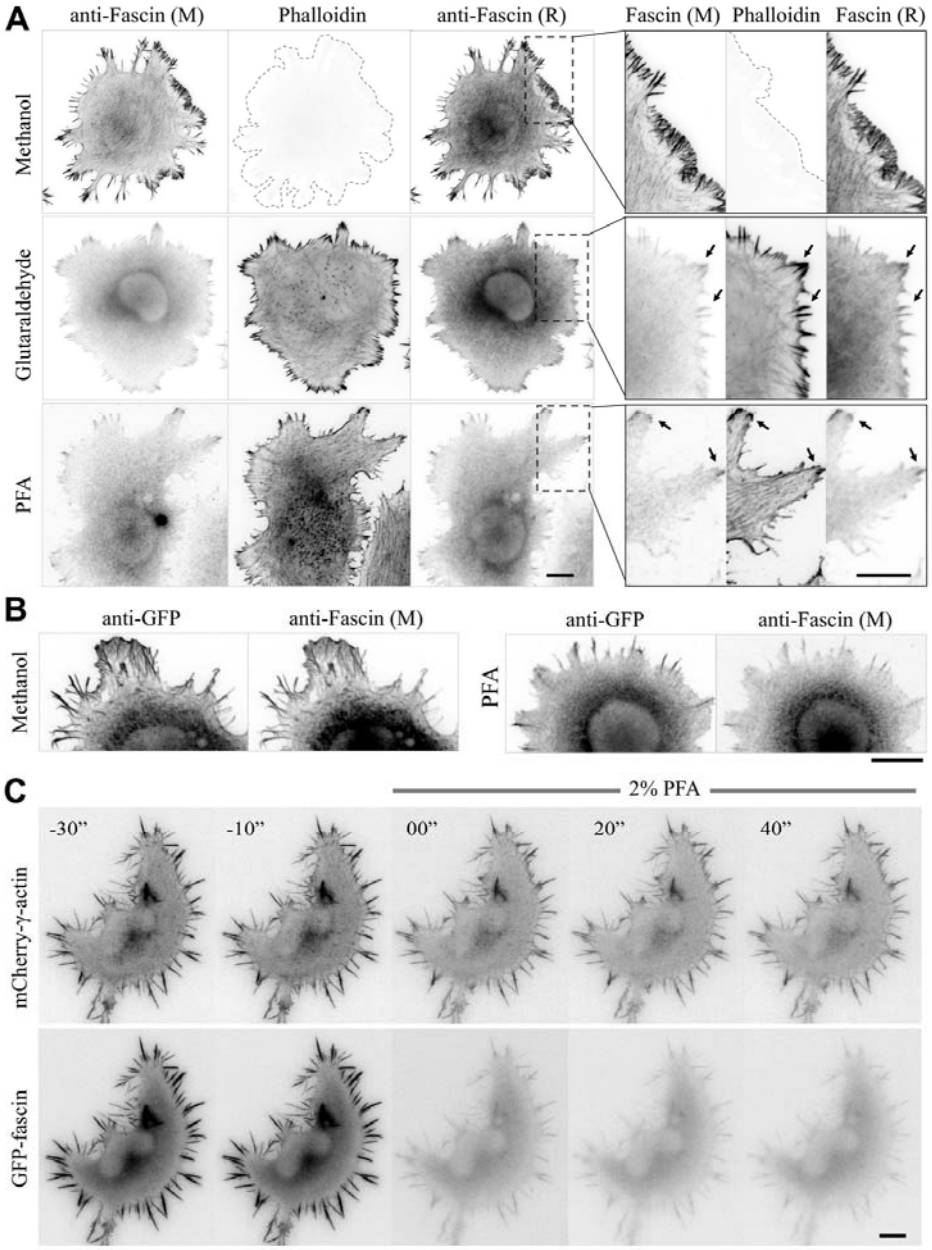

Figure 1. Methanol fixation is required to capture the cellular localization of fascin. (**A**) Representative immunofluorescent images of CAD cells fixed with 100% cold methanol (top row), 2% glutaraldehyde (middle row), or 4% PFA (bottom row). Cells were stained with mouse (M) anti-fascin, rabbit (R) anti-fascin, and phalloidin-AlexaFluor546. Regions enclosed by dashed rectangles are shown at a higher magnification on the right, highlighting the actin-rich lamellipodia and filopodia. Arrows highlight weak fascin signals remaining after aldehyde fixation. (**B**) Representative images of CAD cells expressing GFP-fascin for approximately 24 hours and fixed with either 100% cold methanol (left panels) or 4% PFA (right panels). Cells were stained with mouse (M) anti-Fascin and rabbit anti-GFP. (**C**) Images showing live CAD cells co-expressing GFP-fascin and mCherry-γ-actin, before and after fixation with 2% PFA (added at 0" seconds). Time shown in seconds (total duration 70 seconds). Scale bars: 10 μm.

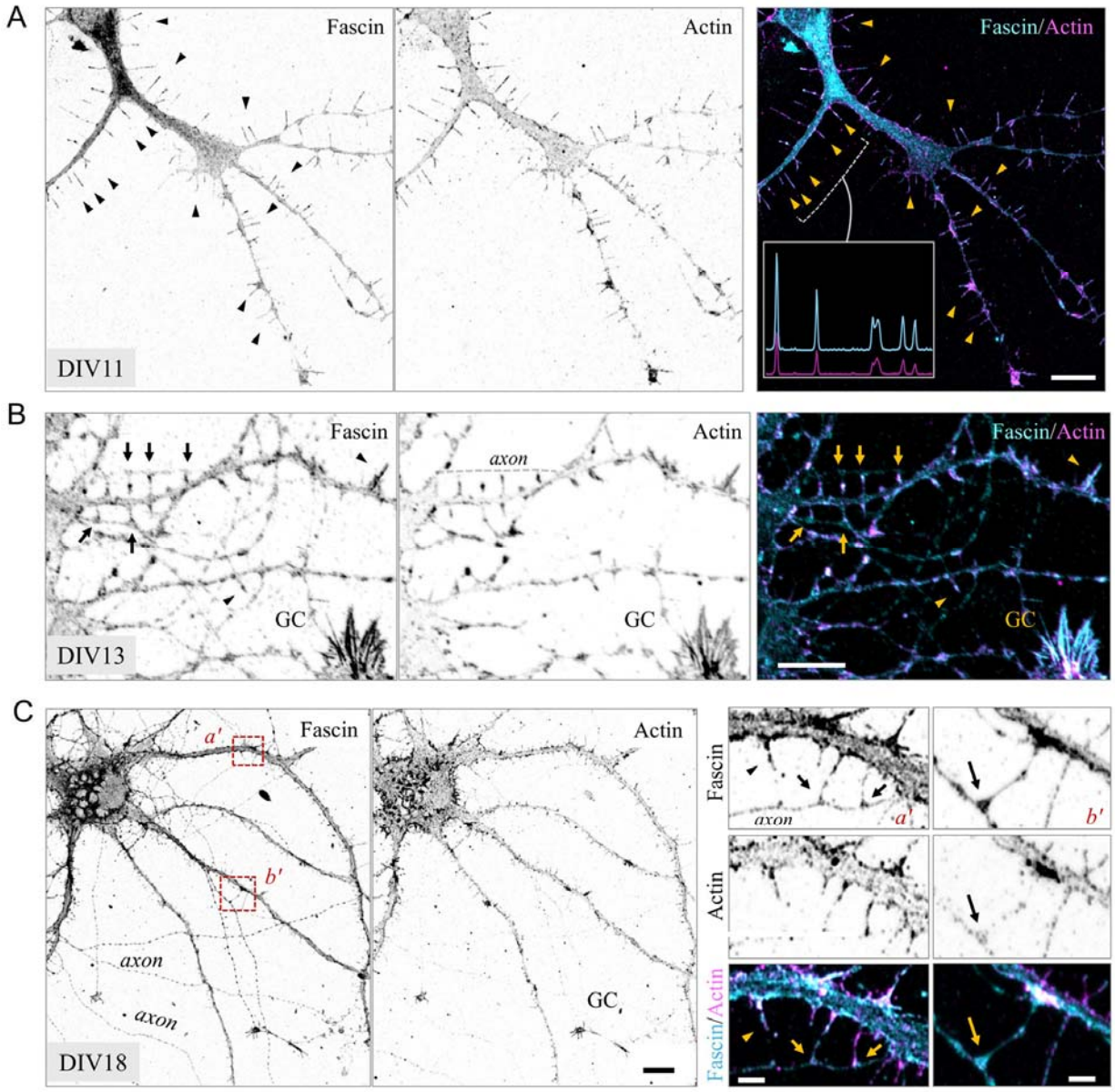

Figure 2. Fascin localizes to dendritic filopodia and immature spine-like protrusions during neuronal development. (**A**) Representative images of low-density cultured hippocampal neurons at DIV11 fixed with 100% cold methanol and labelled for endogenous fascin (cyan) and actin (magenta). Inset in right panel is a linescan showing correlation of fascin and actin levels across multiple filopodia from highlighted region. Arrowheads highlight filopodia with high fascin enrichment. Scale bar = 10 µm. (**B**) Representative images of low-density cultured hippocampal neurons at DIV13 neurons fixed and stained as above. Arrows highlight nascent spines with slightly enlarged heads and fascin enrichment that are in contact with axons. GC: axonal growth cone. Scale bar = 10 µm. (**C**) Representative images of DIV18 neurons fixed and stained as above. Panels on right represent high magnification of corresponding boxed regions from left. Arrows highlight spines with enlarged heads, and arrowheads highlight filopodia. Left scale bar = 10 µm, right scale bars = 2 µm.

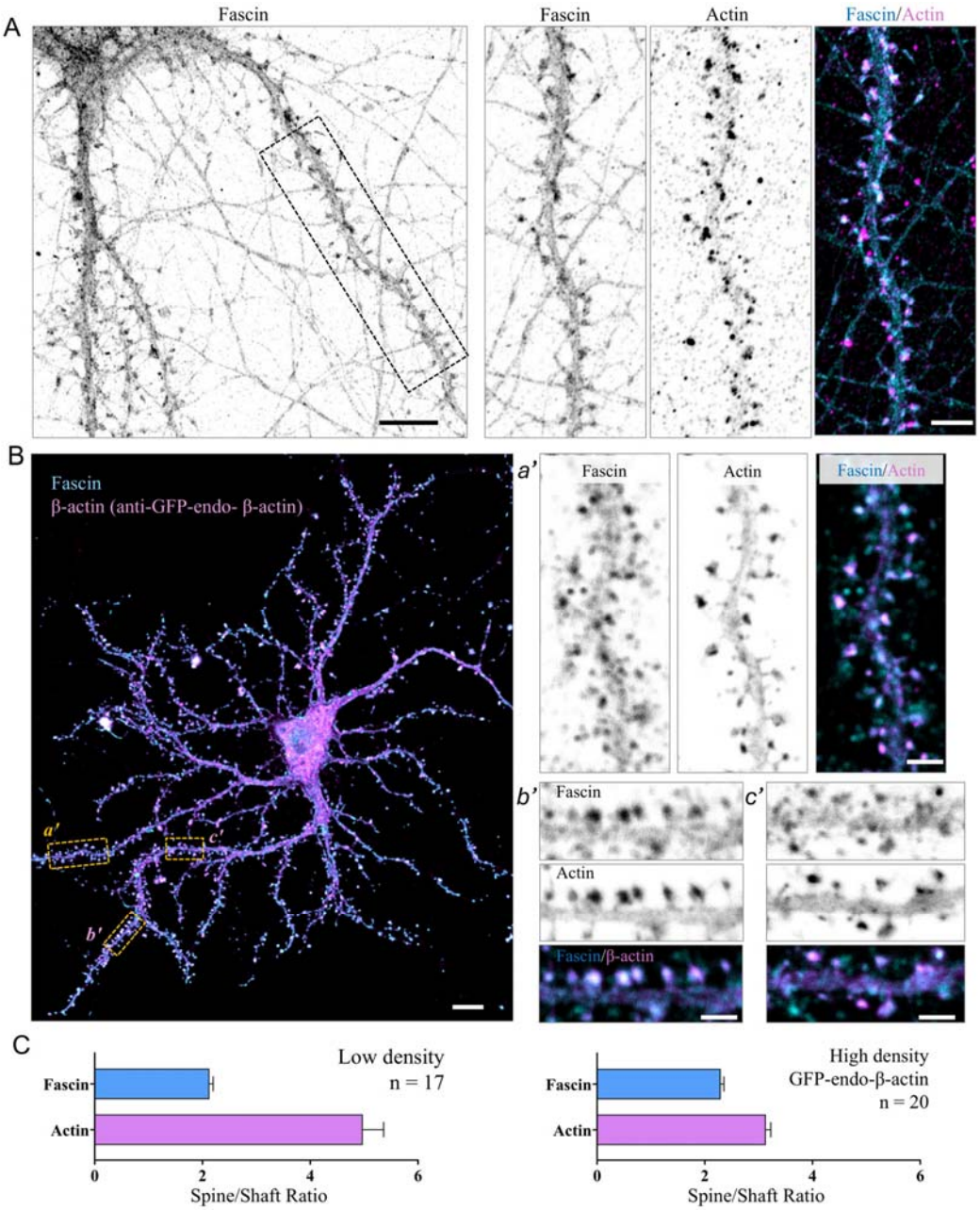

Figure 3. Fascin is enriched in mature dendritic spines. (**A**) Representative images of low-density cultured hippocampal neurons at DIV28 fixed with 100% cold methanol and labelled for endogenous fascin (cyan) and actin (magenta). Left scale bar = 10 µm, right scale bar = 5 µm. (**B**) Representative image of a neuron from high-density hippocampal culture expressing GFP-tagged endogenous β-actin, fixed with 100% cold methanol at DIV28, and labelled for fascin (cyan) and GFP (magenta). GFP-β-actin signal was used as mask to isolate individual neuron from neighboring cells. Right, high magnification panels of boxed regions from image on left. Left scale bar = 10 µm, right scale bars = 2 µm. (**C**) Quantification of fascin enrichment in dendritic spines. Graphs show the ratio of fascin or β-actin fluorescence intensity in spine heads compared to the intensity of an equal-sized area of the neighboring dendritic shaft. *n* = fields of view, representing >200 spines from low density cultures and >500 spines from high density cultures, from 3 independent cultures. Error bars represent SEM.

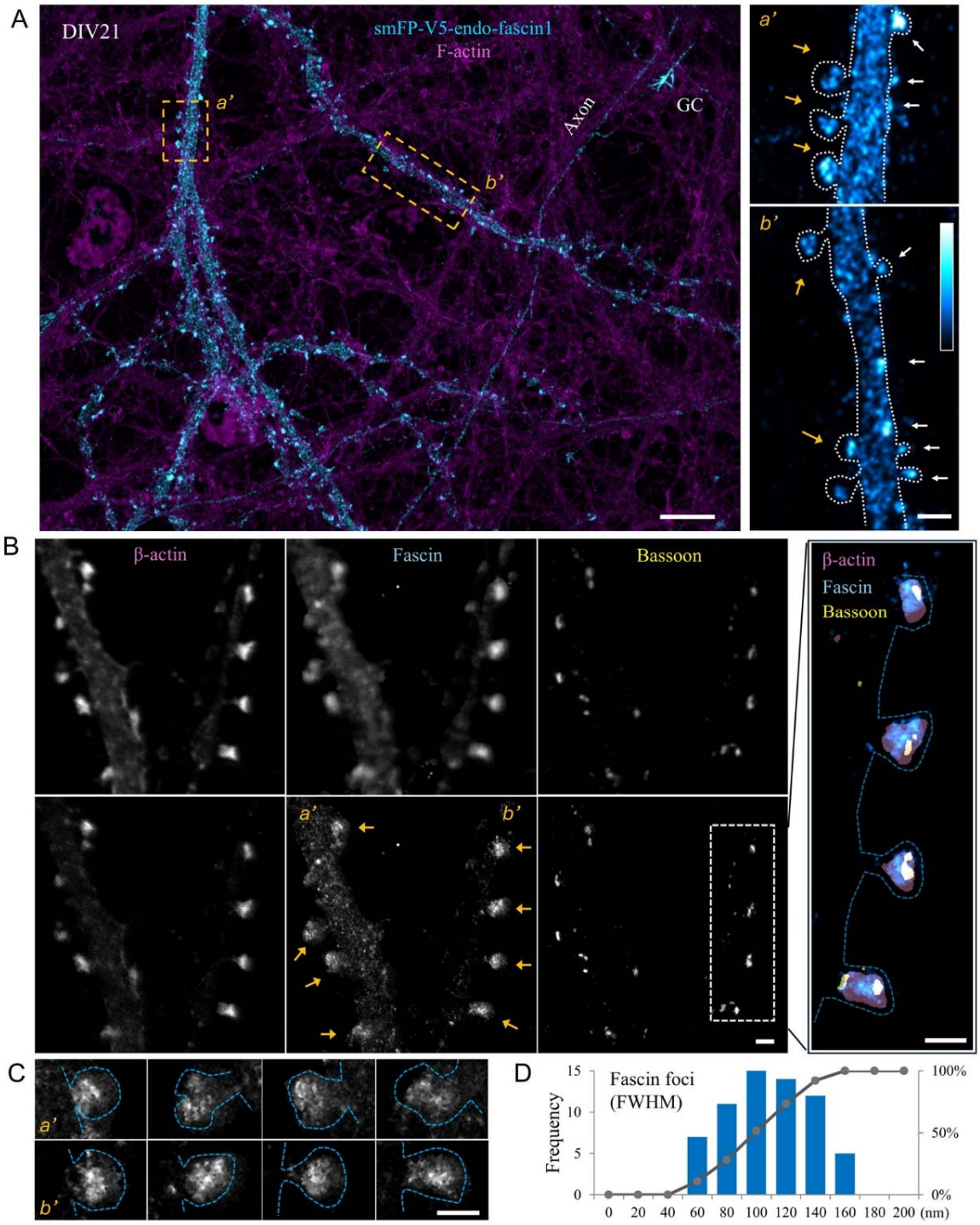

Figure 4. Fascin is enriched in dendritic spine heads as discrete nanoscale foci. (**A**) Representative images of hippocampal neurons at DIV21 with endogenous fascin1 tagged by CRISPR-mediated knock-in of smFP-V5 (cyan). The left panel shows a portion of the dendritic arbor of a neuron expressing smFB-V5-fascin1 (cyan) among the high-density hippocampal culture (immunofluorescently labeled for actin, magenta). Fascin signals are present in dendritic arbors and enriched in dendritic spines, as well as an axonal growth cone (GC). The regions enclosed by dashed rectangles are shown in a high magnification on the right, in which fascin

signals are represented using a cyan hot look-up table. Yellow arrows indicate spines with punctate fascin distribution within the spine heads, whereas white arrows indicate small spines with fascin in their heads. Left scale bar = 10 μm, right scale bars = 2 μm. (**B**) Representative confocal (top row) and STED (bottom row) images of high-density hippocampal cultures expressing GFP-tagged endogenous β-actin, fixed at DIV25 with 100% cold methanol, and triple stained for fascin (cyan), β-actin (magenta), and bassoon (yellow). GFP-β-actin signal was used as mask to isolate individual neurons from neighboring cells. Fascin appears as discrete foci within actin-rich spine heads (arrows), but not in spine necks. A portion of the dendrite (dashed rectangle) is shown on the right, in a higher magnification with three channels merged. Scale bars = 1 μm. (**C**) High magnification images of individual spines in (B) showing punctate fascin distribution (spines outlined in blue). Scale bar = 1 μm. (**D**) Histogram showing width of individual fascin foci in spine heads, assigned within 20 nm bins. Gray bar shows accumulated frequency of foci width. A total of 6 STED images and more than 30 spines were analyzed.

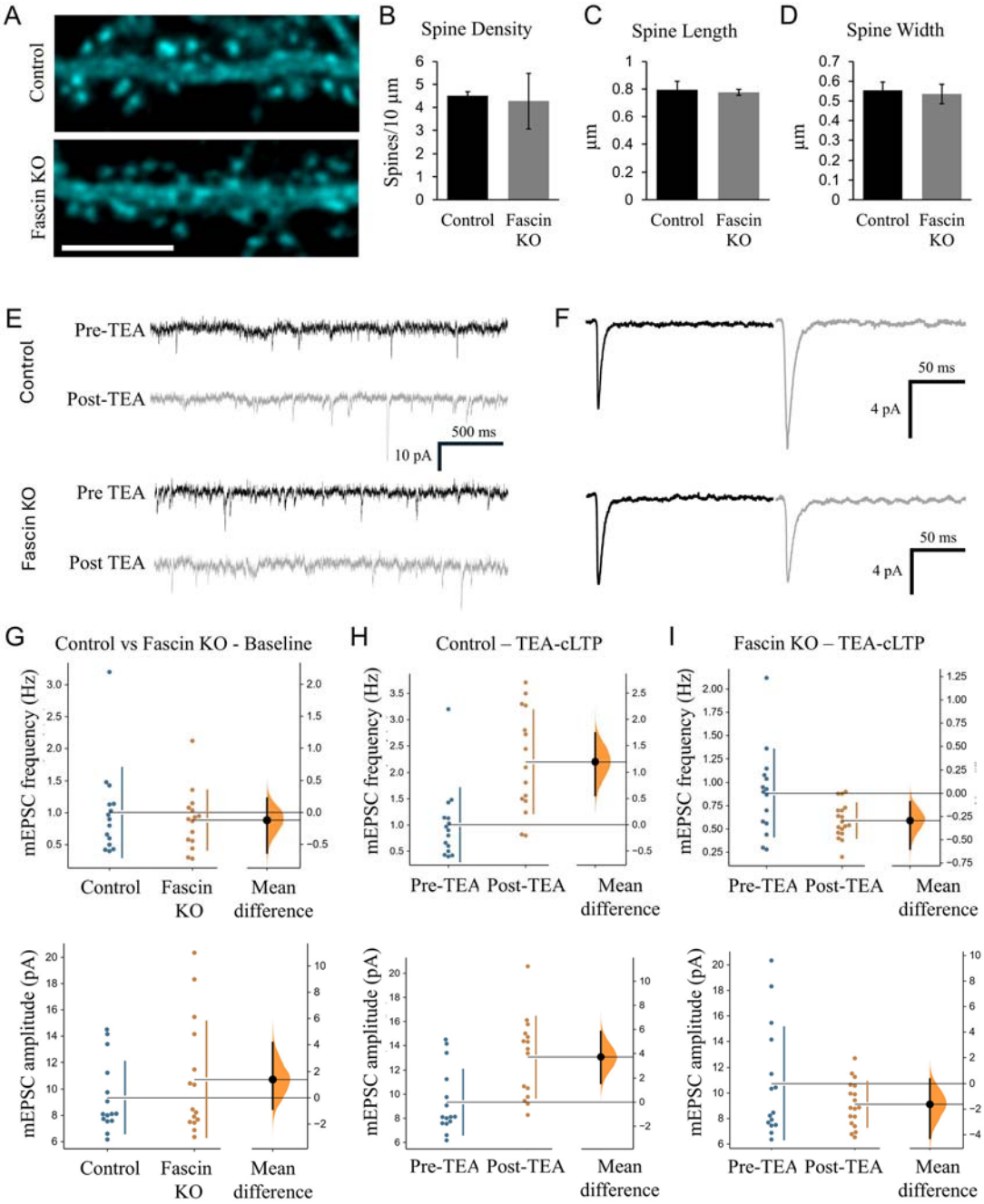

Figure 5. Fascin is required for synaptic potentiation in mature hippocampal neurons. (**A**) Representative images of dendritic spines from control (3xgRNA-KO template) or fascin KO (3xgRNA-KO-Fascin1) high-density hippocampal neurons at DIV25-28. Co-expressed smFP is used to visualize spine morphology. Scale bar = 5 µm. (**B-D**) Plots show no differences in spine density, length, or width between control and fascin KO cells under basal conditions (not significant by unpaired student's *t*-test). Error bars are ± SEM. (**E**) Representative sample traces of mEPSCs from whole-cell patch-clamp recordings of control and fascin KO before and after application of 25 mM TEA. (**F**) Average mEPSC waveforms before (black) and after (gray) TEA application in control (top) and fascin1 KO (bottom) neurons. (**G-I**) Gardner-Altman estimation plots showing that the differences in mEPSC amplitude (top) and amplitude (bottom) between

the control (N=23) and fascin KO (N=15) groups. (G) The baseline synaptic transmission was not affected by fascin KO, as the unpaired mean differences for the frequency and amplitude are 0.387 Hz (95% confidence interval (CI), -0.13, 1.15) and 0.694 pA (95% CI, -1.25, 2.77). P values of the two-sided permutation *t*-test on the frequency and amplitude are 0.25 and 0.52, respectively. (H) TEA-cLTP significantly increased the frequency and amplitude of synaptic transmission in the control group. The unpaired mean differences before and after TEA treatment are 1.06 Hz (95% CI, 0.503, 1.6) and 2.55 pA (95% CI, 0.639, 4.61). P values of the two-sided permutation *t*-test are 0.0006 and 0.03, respectively. (I) TEA-cLTP did not increase, but decreased, the frequency and amplitude of synaptic transmission in the fascin KO group. The unpaired mean differences before and after TEA treatment are -0.935 Hz (95% CI, -1.59, -0.466) and -2.08 pA (95% CI, -3.96, -0.478). P values of the two-sided permutation *t*-test are 0.04 and 0.0004, respectively.

Supplemental figures (S1-S3)

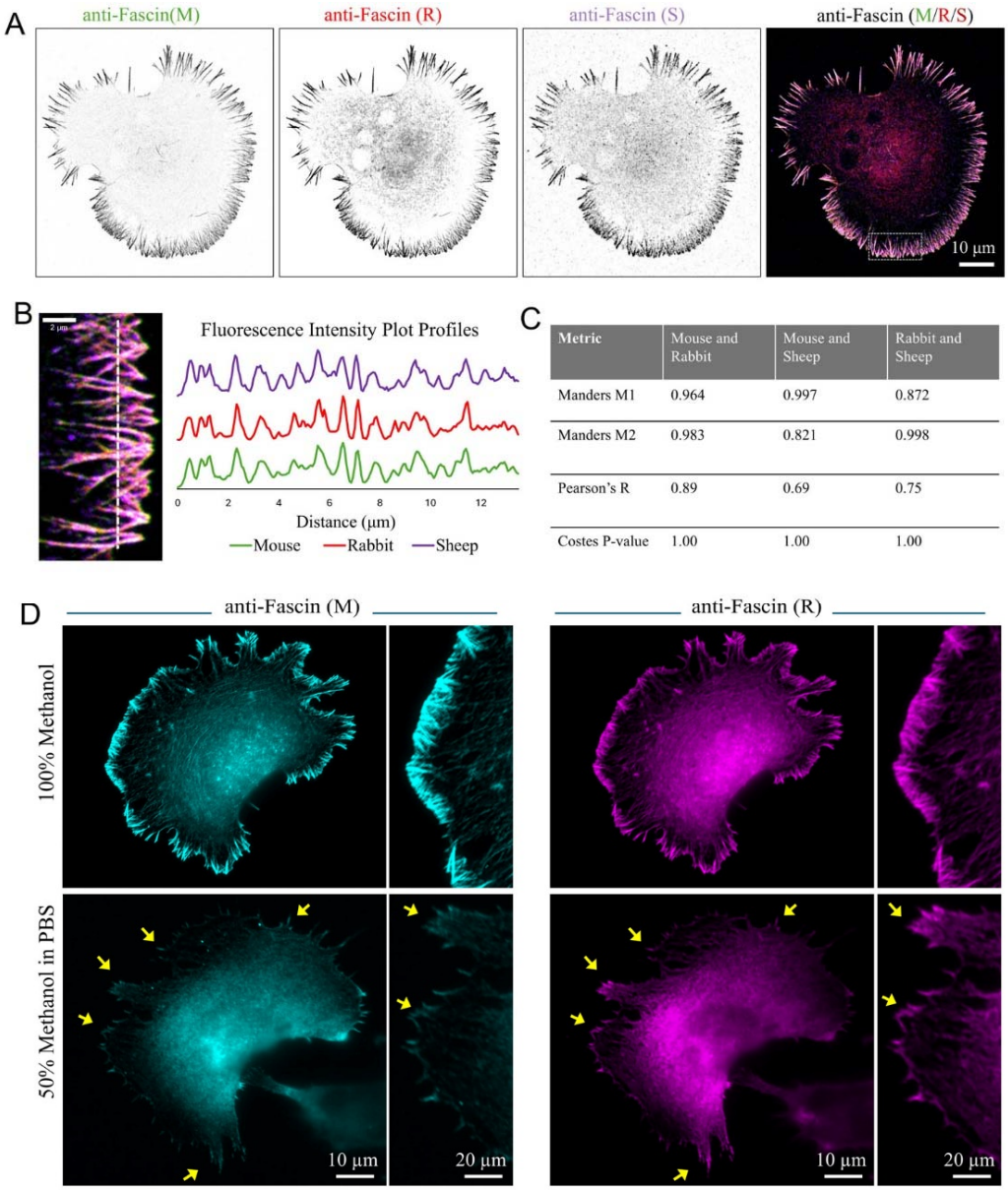

Metric	Mouse and Rabbit	Mouse and Sheep	Rabbit and Sheep
Manders M1	0.964	0.997	0.872
Manders M2	0.983	0.821	0.998
Pearson's R	0.89	0.69	0.75
Costes P-value	1.00	1.00	1.00

Figure S1. Fascin localization after methanol fixation is detected with multiple antibodies. (A) Representative images of CAD cells fixed with 100% cold methanol (−20 °C) and stained with three independent anti-fascin antibodies (raised in mouse (M), rabbit (R), and sheep(S)). (B) Left, magnified image from the boxed region of (A), showing essentially the same fascin enrichment pattern in lamellipodia and filopodia using three independent antibodies. Right, fluorescence intensity profiles corresponding to the dotted white line from image on the left. (C) Quantification of colocalization, analyzed for each pairing of anti-fascin antibodies. (D) Fixation with 50% methanol compromises fascin labeling, compared to fixation with 100% methanol. Representative images of CAD cells fixed with either 100% or 50% cold methanol (−20 °C) and stained with mouse (M) anti-fascin and rabbit (R) anti-fascin antibodies.

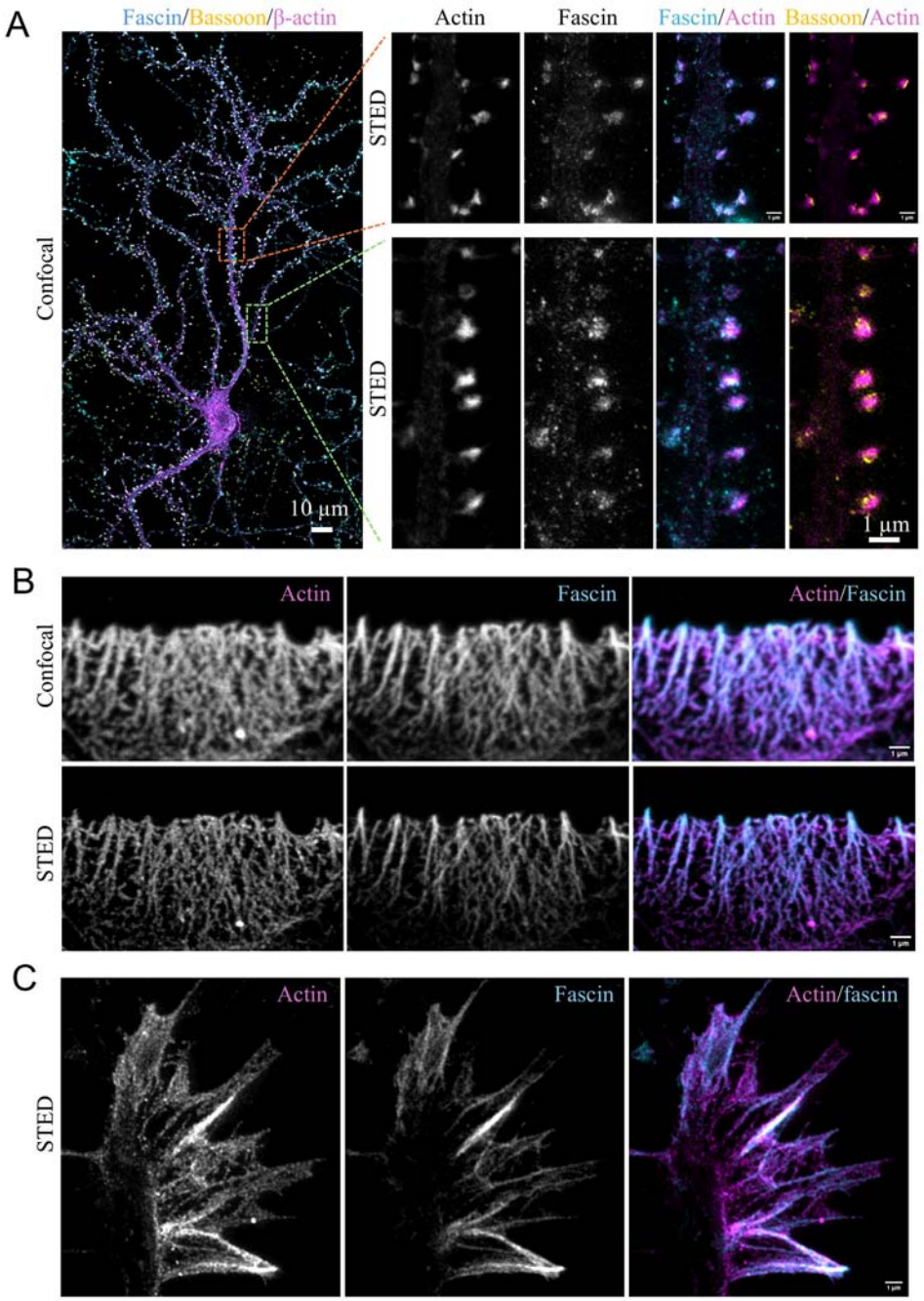

Figure S2. STED imaging of fascin. (A) Representative confocal image of a DIV25 hippocampal neuron expressing GFP-tagged endogenous β-actin, fixed with 100% cold methanol, and labeled with mouse anti-Bassoon, rabbit anti-GFP, and sheep anti-fascin antibodies. Right, STED images of boxed regions from merged image on left, showing fascin foci in dendritic spine heads. (B) Representative confocal and STED images of CAD cell lamellipodia, labelled for endogenous fascin (cyan) and actin (magenta), showing continuous fascin staining pattern along F-actin bundles. (C) Representative STED images of growth cones from primary hippocampal neurons, labelled for endogenous fascin (cyan) and actin (magenta), showing continuous fascin staining pattern along F-actin bundles.

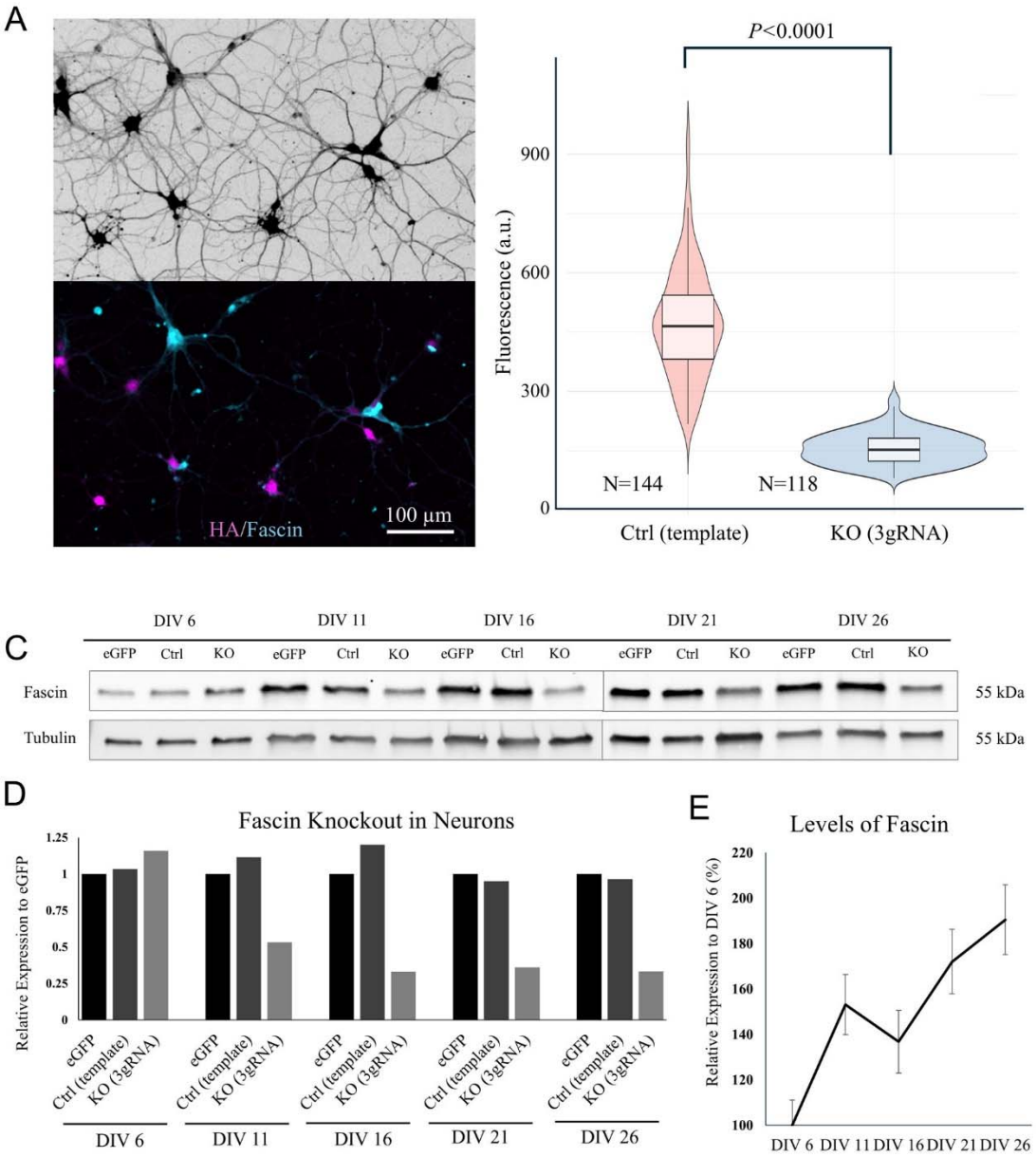

Figure S3. Fascin1 KO validation in hippocampal neurons. (A) Representative immunofluorescence images of methanol-fixed DIV25 hippocampal neurons that were infected on DIV 5 with AAV to express Cas9 and either control (3xgRNA-KO template) or fascin KO (3xgRNA-KO-Fascin1), both of which co-express smFP-HA. Methanol-fixed cells were immunostained for HA to identify transduced cells (magenta) and evaluate fascin levels (cyan). Fascin immunoreactivity is absent in HA-positive fascin KO neurons. (B) Violin and box plot showing the loss of fascin fluorescence intensity in KO cells relative to control neurons. N = number of cells analyzed from 3 separate cultures. (C) Representative western blots showing the levels of fascin and tubulin (used as a loading control) at various times post AAV infection (i.e. DIV 5). (D) Analysis of western blots, showing the effective KO of fascin 12 days post-AAV infection. For each timepoint, samples were normalized to tubulin loading control, and fascin levels in control and KO cells were presented relative to eGFP-expressing neurons. n = 3 separate neuronal cultures. (E) Quantification of fascin levels during primary neuron development. Fascin levels were normalized to tubulin, and presented relative to the initial DIV6 timepoint. Error bars are ± SEM.